Structure and Magnetic Properties of Sr_2CoWO_6: An Ordered Double Perovskite Containing Co^{2+}(HS) with Unquenched Orbital Magnetic Moment

M. C. Viola,[†] M. J. Martínez-Lope,[‡] J. A. Alonso,[‡] J. L. Martínez,[‡] J. M. De Paoli,[§] S. Pagola,[§] J. C. Pedregosa,[†] M. T. Fernández-Díaz,[||] and R. E. Carbonio*[,§]

Area de Química General e Inorgánica "Dr. Gabino F. Puelles", Departamento de Química, Facultad de Química, Bioquímica y Farmacia, Universidad Nacional de San Luis, Chacabuco y Pedernera, 5700 San Luis, Argentina, Instituto de Ciencia de Materiales de Madrid, C.S.I.C., Cantoblanco, E-28049 Madrid, Spain, Instituto de Investigaciones en Físico Química de Córdoba (INFIQC), Departamento de Fisicoquímica, Facultad de Ciencias Químicas, Universidad Nacional de Córdoba, Ciudad Universitaria, 5000 Córdoba, Argentina, and Institut Laue-Langevin, B.P. 156, F-38042 Grenoble Cedex 9, France

Received August 19, 2002. Revised Manuscript Received February 24, 2003

Sr_2CoWO_6 perovskite has been prepared in polycrystalline form by solid-state reaction at 1150 °C. This material has been studied by high-resolution synchrotron X-ray and neutron powder diffraction (NPD), magnetic measurements, and differential scanning calorimetry (DSC). At room temperature, the crystal structure is tetragonal, space group $I4/m$, with $a =$ 5.58277(1) Å and $c = 7.97740(1)$ Å. The structure contains alternating CoO_6 and WO_6 octahedra, tilted in anti-phase by 7.24° in the basal ab plane along the [001] direction of the pseudocubic cell. This corresponds to the $a^0a^0c^-$ Glazer's notation as derived by Woodward for 1:1 ordering of double perovskites, consistent with space group $I4/m$. DSC and NPD measurements as a function of temperature indicate a structural transition from tetragonal to monoclinic (space group $P2_1/n$) at 260 K. At 2 K the cell parameters are $a = 5.61267(8)$ Å, $b = 5.58753(8)$ Å, $c = 7.8994(1)$ Å, and $\beta = 90.041(3)°$. The structure contains alternating CoO_6 and WO_6 octahedra, tilted in-phase by 4.77° along the [001] direction of the pseudocubic cell and in anti-phase by 5.82° along the [010] and [100] directions. This corresponds to the $a^-a^-c^+$ Glazer's notation as derived by Woodward for 1:1 ordering in double perovskites, consistent with space group $P2_1/n$. Magnetic and neutron diffraction measurements indicate an antiferromagnetic ordering below $T_N = 24$ K. The magnetic moment calculated through the linear fit of the Curie−Weiss law at high temperatures (5.20 μ_B) indicates that the orbital contribution is unquenched at high temperatures, which is consistent with high-spin Co^{2+} ($^4T_{1g}$ ground state) in a quasi-regular octahedral environment. As prepared, the sample is an electrical insulator. Magnetic and electrical properties and bond valence sums are consistent with the electronic configuration $Co^{2+}(3d^7)-W^{6+}(5d^0)$.

Introduction

Perovskite oxides of the transition elements have been studied extensively since they present interesting and sometimes unusual magnetic and transport properties. Well-known examples are the superconducting cuprates and the mixed-valence manganese perovskites exhibiting colossal magnetoresistance (CMR). The discovery of CMR has stimulated the enthusiasm of solid-state chemists and physicists since this effect is of technological interest for the detection of magnetic fields in magnetic memory devices.[1] Materials with substantially higher T_C must be developed to operate in a useful temperature range around room temperature (RT).

Recently, some members of the family of double perovskites of composition $A_2BB'O_6$ (A = alkali earths, B and B′= transition metals) have been proposed as half-metallic ferromagnets (best described as ferrimagnets), with T_C's well above RT, as an alternative to perovskite manganites.[2−6] The revival of interest in this family was triggered by a report on Sr_2FeMoO_6,[2] demonstrating that in the electronic structure only minority spins are present at the Fermi level: this material was shown to exhibit intrinsic tunneling-type magneto-

* To whom correspondence should be addressed. Fax: +54-351-433-4188. E-mail: carbonio@mail.fcq.unc.edu.ar.
[†] Universidad Nacional de San Luis.
[‡] Instituto de Ciencia de Materiales de Madrid, C.S.I.C.
[§] Universidad Nacional de Córdoba.
[||] Institut Laue-Langevin.

(1) Rao, C. N. R., Raveau, B., Eds. *Colossal magnetoresistance and other related properties in 3d oxides*; World Scientific: Singapore, 1998.
(2) Kobayashi, K.-I.; Kimura, T.; Sawada, H.; Terakura, K.; Tokura, Y. *Nature* **1998**, *395*, 677.
(3) García-Landa, B.; Ritter, C.; Ibarra, M. R.; Blasco, J.; Algarabel, P. A.; Mahendiran, R.; García, J. *Solid State Commun.* **1999**, *110*, 435.
(4) Maignan, A.; Raveau, B.; Martin, C.; Hervieu, M. *J. Solid State Chem.* **1999**, *144*, 224.
(5) Kobayashi, K. L.; Kimura, T.; Tomioka, Y.; Sawada, H.; Terakura, K.; Tokura, Y. *Phys. Rev. B* **1999**, *59*, 11159.
(6) Kim, T. H.; Uehara, M.; Cheong, S. W.; Lee, S. *Appl. Phys. Lett.* **1999**, *74*, 1737.

10.1021/cm0208455 CCC: $25.00
Published on Web 04/15/2003

resistance (TMR) at RT.[2,6] In a simple picture, FeO_6 and MoO_6 octahedra alternate along the three directions of the crystal structure of Sr_2FeMoO_6; the ferrimagnetic structure can be described as an ordered arrangement of parallel Fe^{3+} ($S = {}^5/_2$) magnetic moments, antiferromagnetically coupled with Mo^{5+} ($S = {}^1/_2$) spins.

Further studies on other members of the $A_2BB'O_6$ family seem to indicate that the occurrence of CMR and/or TMR properties is a common feature in some of them. The A = Ca, Ba analogues of the Sr_2FeMoO_6 were also found to exhibit semimetallic and ferromagnetic properties.[4,7−9] As well, A_2FeReO_6 (A = Ca, Sr, Ba) presents[10,11] a half metallic ground-state concomitant with the ferrimagnetic coupling of Fe^{3+} and Re^{5+} ($5d^2$, $S = {}^2/_2$) magnetic moments, and show CMR and/or TMR at RT. These results are encouraging for exploration of other prospective half-metallic compounds such as CMR and/or TMR materials with sufficiently large effect at low magnetic fields, in ferromagnetic compounds with T_C's as close as possible to RT.

We recently reported the induction of CMR in Sr_2CoMoO_6[12] upon chemical reduction, via topotactical removal of oxygen atoms. The structure of the stoichiometric sample was described as tetragonal, space group $I4/m$, with $a = 5.56503(5)$ Å and $c = 7.94810(8)$ Å. It was reported to be antiferromagnetic with $T_N = 37$ K. The most remarkable result was the induction of CMR as high as 30% at 12 K for $H = 9$ T.

The W analogue of Sr_2CoMoO_6 has attracted our attention. This double perovskite was first studied in the 1960s.[11,13] It was reported to be an antiferromagnet with $T_N = 22$ K.[13,14] Its structure was previously described as a tetragonal distortion of perovskite,[15] with unit-cell parameters $a = b = 3.957$ Å and $c = 3.989$ Å at room temperature, assuming a random distribution of Co and W atoms at the 1b sites of the space group $P4mm$.

In the present work we describe the synthesis of Sr_2CoWO_6 prepared by a solid-state reaction and the results of Rietveld analysis of synchrotron X-ray diffraction (SXRPD) and neutron powder diffraction (NPD) data on a well-crystallized sample. The structure has been revisited: we report complete structural data for this double perovskite, which contains two crystallographically independent sites for Co and W cations. Low-temperature NPD data, differential scanning calorimetry (DSC) results, and magnetic properties are also discussed.

Experimental Section

Sr_2CoWO_6 was prepared as a yellow polycrystalline powder by solid-state reaction. Stoichiometric amounts of analytical-grade $Sr(CO_3)$, Co_2O_3, and WO_3 were mixed, ground, and treated at 900 °C for 6 h in air. The resulting powder was reground and calcined at 1150 °C for 24 h in air. The initial structural identification and characterization of the sample was carried out by laboratory X-ray powder diffraction (XRD) (Cu Kα, $\lambda = 1.5406$ Å). For the structural refinement of Sr_2CoWO_6, synchrotron X-ray powder diffraction (SXRPD) and neutron powder diffraction (NPD) data were used. A SXRPD pattern was collected at room temperature (RT) at the SUNY X3B1 beamline of the N.S.L.S., Brookhaven National Laboratory, USA ($\lambda = 1.150046$ Å). The 2θ range was 2° up to 48° with increments of 0.01° and the counting time was 4 s/step. The high-resolution NPD patterns were collected at RT and 2 K at the D2B diffractometer (ILL, Grenoble, France). The high-flux mode was used, with a wavelength of 1.594 Å, selected from a Ge monochromator. About 8 g of sample was placed in a vanadium can; the counting time was 3 h. The variable temperature NPD patterns in the range 2−300 K were collected at the D20 high-flux neutron diffractometer (ILL, Grenoble, France), using a wavelength of 2.42 Å. Once cooled to 2 K, the sample was heated at 1K min^{-1} and the patterns were sequentially collected with counting times of 2 min.

The program FULLPROF[16] was used to refine the crystal structure by the Rietveld method. A pseudo-Voigt shape function was always adequate for obtaining good fits for NPD and a pseudo-Voigt function convoluted with an axial divergence asymmetry function[17] was used for the SXRPD data.

Attempts to refine simultaneously NPD and SXRPD gave standard deviations and R_{Bragg} factors larger than those obtained with NPD or SXRPD separately. For this reason we decided to refine the structure with NPD data, fixing the cell parameters and Co/W mixing parameters to their values obtained from the SXRPD refinement and to refine the neutron wavelength.

The following parameters were refined from the SXRPD data: scale factor, background coefficients, zero-point error, unit-cell parameters, pseudo-Voigt corrected for asymmetry parameters, positional coordinates, an overall isotropic thermal factor, and antisite disorder of Co/W.

The following parameters were refined from the NPD data: scale factor, background coefficients, zero-point error, neutron wavelength (cell parameters and Co/W mixing parameters were fixed to their values obtained from SXRPD data for the RT NPD data), pseudo-Voigt corrected for asymmetry parameters, positional coordinates, isotropic thermal factors, and O occupancies. The coherent scattering lengths for Sr, Co, W, and O were 7.02, 2.49, 4.86, and 5.80 fm, respectively.

The dc magnetic susceptibility was measured with a commercial SQUID magnetometer on powdered samples, in the temperature range 1.5−400 K. Transport measurements were performed by the conventional four-probe technique in a PPMS system from Quantum Design, in sintered pellets of $10 \times 3 \times 2$ mm^3. Differential scanning calorimetry (DSC) measurements were performed in a Seiko U system, in the temperature range from 223 to 773 K. The heating rate was 10 °C min^{-1}, using about 70 mg of sample.

Results

Structural Refinement. *SXRPD Data.* The refined SXRPD data of Sr_2CoWO_6 (space group $I4/m$) at RT are shown in Figure 1. The pattern is characteristic of a perovskite structure, showing superstructure reflections corresponding to the Co/W ordering and a tetragonal distortion. Sr_2WO_5 (space group $Pnma$) and $SrWO_4$ (space group I_1/a) were included as minor impurity

(7) Alonso, J. A.; Casais, M. T.; Martínez-Lope, M. J.; Velasco, P.; Muñoz, A.; Fernández-Díaz, M. T. *Chem. Mater.* **2000**, *12*, 161.
(8) Borges, R. P.; Thomas, R. M.; Cullinan, C.; Coey, J. M. D.; Suryanarayan, R.; Ben-Dor, L.; Pinsard-Gaudart, L.; Revcolevschi, A. *J. Phys.: Condens. Matter* **1999**, *11*, L445.
(9) Ritter, C.; Ibarra, M. R.; Morellón, L.; Blasco, J.; García, J.; De Teresa, J. M. *J. Phys.: Condens. Matter* **2000**, *12*, 8295.
(10) Prellier, W.; Smolyaninova, W.; Bisbas, A.; Galley, C.; Greene, R. L.; Ramesha, K.; Golapakrishnan, J. *J. Phys.: Condens. Matter* **2000**, *12*, 965.
(11) Galasso, F. *Structure, Properties and Preparation of Perovskite-Type Compounds*; Pergamon Press: Oxford, 1969.
(12) Viola, M. C.; Martínez-Lope, M. J.; Alonso, J. A.; Velasco, P.; Martínez, J. L.; Pedregosa, J. C.; Carbonio, R. E.; Fernández-Díaz, M. T. *Chem. Mater.* **2002**, *14*, 812.
(13) Blasse, G. *Philips Res. Rep.* **1965**, *20*, 327.
(14) Landolt-Börnstein. *Zahlenwerte und Funktionen aus Naturwissenschaften und Tecnik*; Neue serie, Band 4, Teil a; Springer-Verlag: Berlin, 1970.
(15) Kupriyanov, M. F.; Fesenko, E. G. *Kristallografiya* **1962**, *451*, 7.
(16) Rodríguez-Carvajal, J. *Physica B (Amsterdam)* **1993**, *192*, 55.
(17) Finger, L. W.; Cox, D. E.; Jephcoat, A. P. *J. Appl. Crystallogr.* **1994**, *27*, 892.

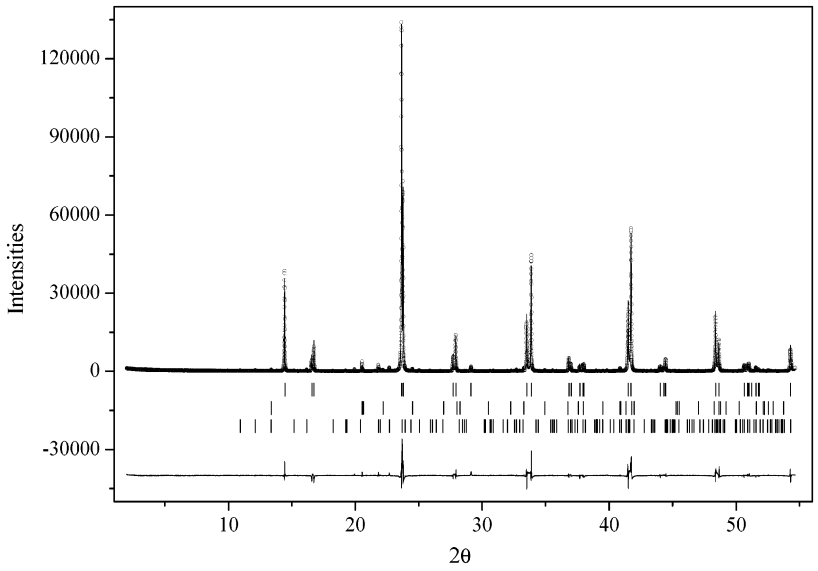

Figure 1. Observed (circles), calculated (full line), and difference (bottom) SXRPD Rietveld profiles for Sr_2CoWO_6 at 298 K. Vertical lines correspond to the Bragg positions for Sr_2CoWO_6 (top) and minor impurity phases (bottom).

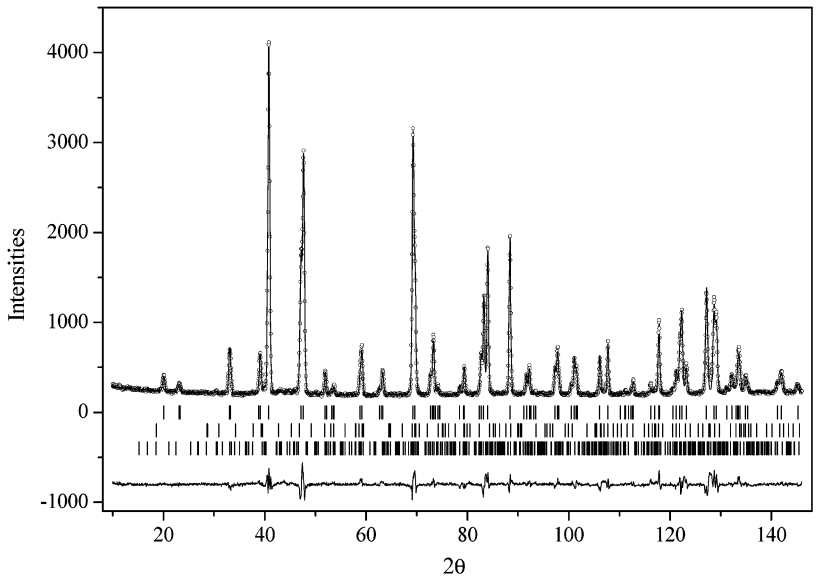

Figure 2. Observed (circles), calculated (full line), and difference (bottom) NPD Rietveld profiles for Sr_2CoWO_6 at 298 K. Vertical lines correspond to the Bragg positions for Sr_2CoWO_6 (top) and minor impurity phases (bottom).

phases in the refinement (1.53 and 1.22%, respectively, were obtained from their scale factors). From this refinement only cell parameters ($a = b = 5.58277(1)$ Å, $c = 7.97740(1)$ Å) and Co/W mixing parameters were obtained to be used as fixed values in the refinements with NPD data at RT. The refinement of the inversion degree led to 4.7% of anti-site disordering.

D2B Room-Temperature NPD Data. The structural refinement from RT high-resolution NPD data was performed in the *I*4/*m* space group (No. 87), $Z = 2$, with unit-cell parameters related to a_0 (ideal cubic perovskite, $a_0 \approx 3.95$ Å) as $a = b \approx \sqrt{2}a_0$, $c \approx 2a_0$. Sr atoms were located at 4d positions, Co/W at 2a/2b sites, and oxygen atoms at 4e and 8h positions. Sr_2WO_5 (space group *Pnma*) and $SrWO_4$ (space group I_1/a) were included as impurity phases in the refinement. An excellent fit was obtained for this model, as shown in Figure 2. As discussed later, refinements were also performed in the *P*4/*mnc* space group; however, *R* values were much larger than those for *I*4/*m*. The oxygen stoichiometry of O1 and O2 was checked by refining their occupancy factors; no oxygen vacancies were found to be present. Table 1a includes the final atomic coordinates and agreement factors after the refinement. A drawing of the structure is shown in Figure 3. The structure contains alternating CoO_6 and WO_6 octahedra, tilted in anti-phase by 7.24° in the basal *ab* plane (along the [001] direction of the pseudocubic cell). This corresponds to the $a^0a^0c^-$ Glazer's notation as derived by Woodward[18] for 1:1 ordering of double perovskites, consistent with space group *I*4/*m*. Table 2a lists the main interatomic distances and angles. Results of the bond valence analysis according to the Brown model[19] are shown in Table 3a. An interesting result of this analysis is that Co is in the +2 oxidation state and W in the +6 oxidation state; this fact will be discussed later.

(18) Woodward, P. M. *Acta Crystallogr. B* **1997**, *53*, 32.
(19) Brown, I. D. *Structure and Bonding in Crystals*; O'Keeffe, M., Navrotsky, A., Eds.; Academic Press: New York, 1981; Vol. 1.

Table 1. Positional Parameters for Sr_2CoWO_6

(a) Tetragonal *I*4/*m* Space Group, $Z = 2$, from NPD Data at 298 K[a]

atom	site	*x*	*y*	*z*	B_{iso}	occ
Sr	4d	0	0.5	0.25	0.86(2)	1
Co	2a	0	0	0	−0.06(8)	0.957(2)[a]
W	2a	0	0	0	−0.06(8)	0.047(2)[a]
Co	2b	0	0	0.5	1.6(2)	0.047(2)[a]
W	2b	0	0	0.5	1.6(2)	0.957(2)[a]
O1	4e	0	0	0.2390(5)	1.33(3)	1
O2	8h	0.2100(3)	0.2734(3)	0	1.00(2)	1

(b) Monoclinic $P2_1/n$ Space Group, $Z = 2$, from NPD Data at 2 K[b]

atom	site	*x*	*y*	*z*	B_{iso}
Sr	4e	0.9979(3)	0.0146(3)	0.2487(7)	0.34(2)
Co	2c	0.5	0	0.5	0.7(2)
W	2d	0.5	0	0	0.06(8)
O1	4e	0.0485(3)	0.4950(5)	0.2601(5)	0.49(5)
O2	4e	0.7187(6)	0.2636(8)	0.0251(7)	0.76(9)
O3	4e	0.2398(6)	0.2240(7)	0.9748(7)	0.43(7)

[a] The unit cell parameters are $a = b = 5.58277(1)$ Å, $c = 7.97740(1)$ Å, $V = 248.634(1)$ Å^3. (Values obtained by refinement of synchrotron data.) $R_p = 4.18\%$, $R_{wp} = 5.74\%$, $R_{exp} = 3.19\%$, $\chi^2 = 3.24$, $R_I = 2.85\%$. [b] The unit cell parameters are $a = 5.61267(8)$ Å, $b = 5.58753(8)$ Å, $c = 7.8994(1)$ Å, $\beta = 90.041(3)°$, $V = 247.733(6)$ Å^3. $R_p = 10.8\%$, $R_{wp} = 9.66\%$, $R_{exp} = 7.41\%$, $\chi^2 = 1.70$, $R_I = 4.17\%$.

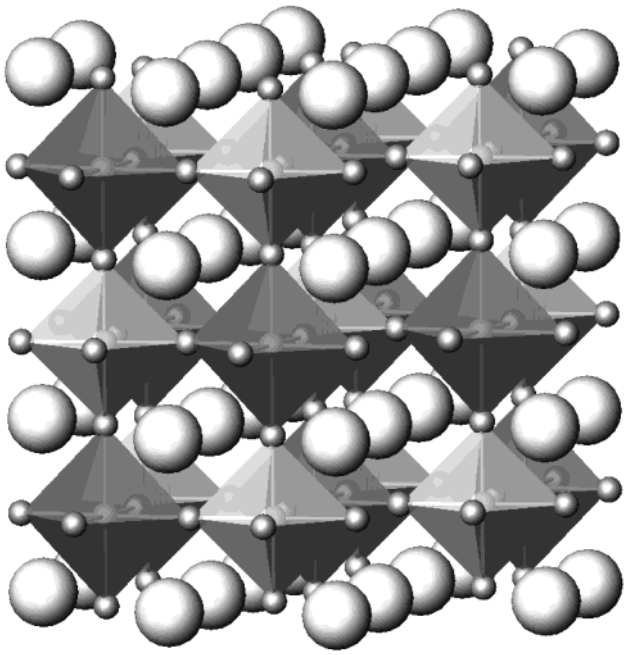

Figure 3. View of the structure of tetragonal Sr_2CoWO_6 at 298 K. *c* axis is vertical; *a* axis is from left to right. Large spheres represent Sr; small spheres represent O; corner-sharing CoO_6 (dark) and WO_6 octahedra are tilted in antiphase along the *c* axis, to optimize Sr−O bond lengths.

D20 Variable Temperature NPD Data. NPD data taken in the 160−300 K temperature range show a tetragonal (high temperature, space group *I*4/*m*) to monoclinic (low temperature, space group $P2_1/n$) transition at ca. 260 K. The main feature of this transition is the appearance (see Figure 4), for the monoclinic phase, of a reflection at 57.8° ($d = 2.50$ Å) corresponding to the (210) and (120) planes. These are systematic absences in the tetragonal *I*4/*m* space group (*hk*0: $(h + k = 2n + 1)$). The refined volume and cell parameters as a function of temperature are shown in Figure 5. A sharp change around 260 K is observed, coincident with the temperature of the phase transition. A monotonic contraction of the unit cell is observed as the temperature decreases.

Table 2. Main Bond Distances (Å) and Selected Angles (deg) for Sr_2CoWO_6

(a) Tetragonal, Determined from NPD Data at 298 K

CoO_6 Octahedron	
$(Co)_{2a}$−O1 (×2)	2.082(4)
$(Co)_{2a}$−O2 (×4)	2.055(2)
⟨Co−O⟩	2.064(3)
WO_6 Octahedron	
$(W)_{2b}$−O1 (×2)	1.906(4)
$(W)_{2b}$−O2 (×4)	1.925(2)
⟨W−O⟩	1.919(3)
Co−O1−W (×2)	180.0
Co−O2−W (×4)	165.52(7)
SrO_{12} Polyhedron	
Sr−O1 (×4)	2.7930(1)
Sr−O2 (×4)	2.988(1)
Sr−O2 (×4)	2.637(1)
⟨Sr−O⟩	2.806(1)

(b) Monoclinic, Determined from NPD Data at 2 K

CoO_6 Octahedron	
$(Co)_{2c}$−O1 (×2)	2.073(4)
$(Co)_{2c}$−O2 (×2)	2.068(4)
$(Co)_{2c}$−O3 (×2)	2.057(4)
⟨Co−O⟩	2.066(3)
WO_6 Octahedron	
$(W)_{2d}$−O1 (×2)	1.914(4)
$(W)_{2d}$−O2 (×2)	1.927(4)
$(W)_{2d}$−O3 (×2)	1.933(4)
⟨W−O⟩	1.925(4)
Co−O1−W (×2)	164.2(2)
Co−O2−W (×2)	164.7(2)
Co−O3−W (×2)	165.9(2)
SrO_{12} Polyhedron	
(Sr)−(O1)	2.919(3)
(Sr)−(O1)	2.701(3)
(Sr)−(O1)	3.069(3)
(Sr)−(O1)	2.549(3)
(Sr)−(O2)	2.740(6)
(Sr)−(O2)	2.577(6)
(Sr)−(O2)	3.103(6)
(Sr)−(O2)	2.799(7)
(Sr)−(O3)	2.810(7)
(Sr)−(O3)	3.094(6)
(Sr)−(O3)	2.583(6)
(Sr)−(O3)	2.725(6)
⟨Sr−O⟩	2.806(5)

Table 3. Bond-Valence Sums Obtained from the Brown Model[19] for Sr_2CoWO_6[a]

(a) Tetragonal, at 298 K

atom	bond-valence sums	atom	bond-valence sums
Sr	2.011(2)	O1	2.02(2)
Co	2.198(6)	O2	2.031(5)
W	5.98(2)		

(b) Monoclinic, at 2 K

atom	bond-valence sums	atom	bond-valence sums
Sr	2.12(1)	O1	2.07(1)
Co	2.184(9)	O2	2.04(1)
W	5.87(3)	O3	2.03(1)

[a] R_{ij} values obtained from ref 20 were as follows: $R_{Sr(II)-O} = 2.118$, $R_{Co(II)-O} = 1.692$, and $R_{W-O} = 1.917$ Å.

Magnetic Structure. The magnetic structure of Sr_2CoWO_6 and its thermal evolution were analyzed from

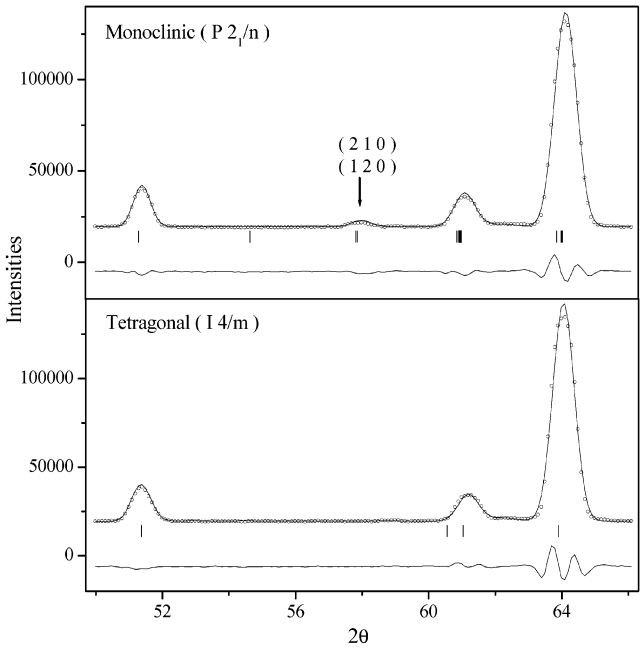

Figure 4. Comparison of refined NPD profiles in the tetragonal (165 K) and monoclinic (298 K) sides.

a set of NPD patterns sequentially collected in the temperature range $2 < T < 140$ K, with $\lambda = 2.42$ Å. On decreasing temperature below 32 K, new reflections appear on positions forbidden for the Bragg reflections in the space group $P2_1/n$. These new peaks correspond to magnetic satellites defined by the propagation vector $\mathbf{k} = (^1/_2, 0, ^1/_2)$. An antiferromagnetic structure was modeled with magnetic moments at the Co positions; after the full refinement of the profile, including the magnetic moment magnitude, a discrepancy factor of $R_{mag} = 6.78\%$ was reached for the 2 K diagram, collected with a longer counting time of 10 min. The best agreement was obtained by considering the magnetic moments aligned along the [110] directions. A view of the magnetic structure is displayed in Figure 6. The proposed magnetic arrangement gives rise to antiferromagnetic couplings between each Co moment and the six nearest neighbors, via −O−W−O− paths. The magnetic structure can be alternately described as an array of ferromagnetic layers of Co moments, perpendicular to the [101] directions, coupled antiferromagnetically. The magnetic structure is stable from 2 K to T_N, as demonstrated in a sequential refinement in the entire available temperature range. The thermal evolution of the ordered magnetic moment on the Co positions is shown in Figure 7. A sharp increase is observed below 32 K, reaching the saturation value of 2.35(3) μ_B at 2 K. This value represents the magnetic moment per Co^{2+} ion in the ordered state and should be associated with the spin-only contribution, although it is lower than the expected value for high-spin Co^{2+} of $3\mu_B$/atom, probably due to covalence effects.

The thermal variation of the unit-cell parameters refined from NPD taken in the 2−140 K temperature range shows a change in slope around 32 K, especially in *b* and *c* (Figure 8). This corresponds to the paramagnetic to antiferromagnetic transition, suggesting a magnetostrictive character for this magnetic transition.

D2B NPD at 2 K. To obtain a good structural refinement of the monoclinic antiferromagnetic phase at 2 K,

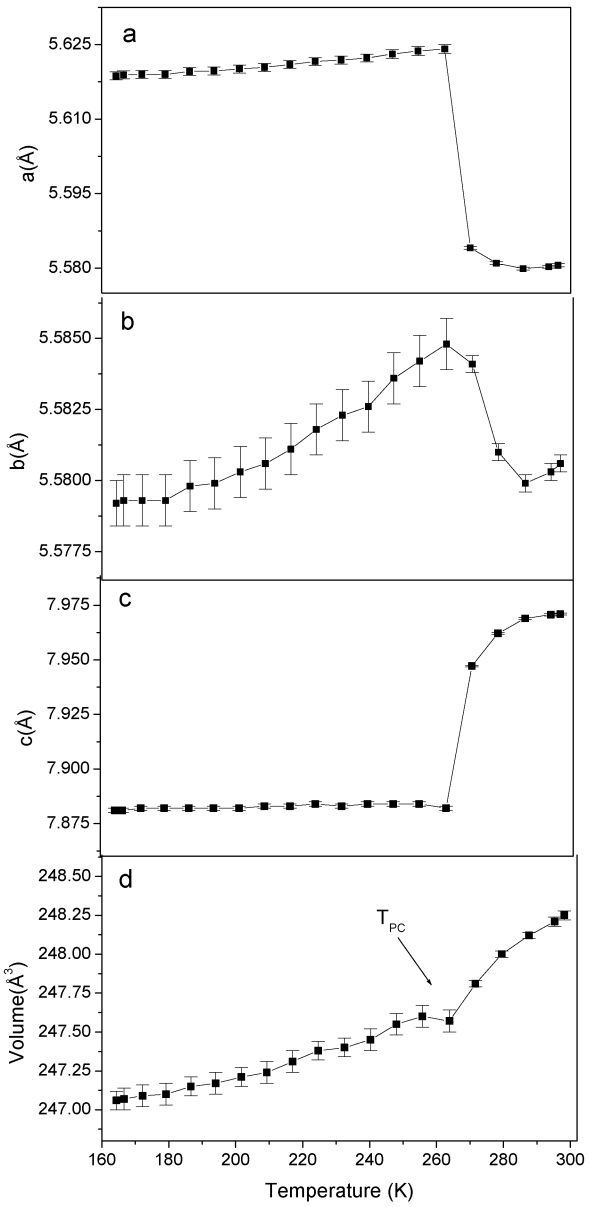

Figure 5. Dependence of volume and cell parameters with temperature in the range 160−300 K. T_{PC} = temperature of phase transition.

measurements at this temperature were performed at the high-resolution D2B powder diffractometer. In the space group $P2_1/n$, Sr atoms are located at 4e positions, Co at 2c, and W at 2d, and the three kinds of independent atomic positions O1, O2, and O3 are placed at 4e sites. The magnetic structure, defined as in the preceding section, was included as a second phase in the refinement. The refined profile is shown in Figure 9 and the final parameters are shown in Table 1b. Table 2b lists the main interatomic distances and angles. Results of the bond-valence analysis according to the Brown model[19] are shown in Table 3b. A drawing of the structure is shown in Figure 10. The structure contains alternating CoO_6 and WO_6 octahedra, tilted in-phase by 4.77° along the [001] direction of the pseudocubic cell and in anti-phase by 5.82° along the [010] and [100] directions. This corresponds to the $a^-a^-c^+$ Glazer's notation[21] as derived by Woodward[18] for 1:1 ordering in double perovskites, consistent with space group $P2_1/n$. The phase transition thus corresponds to the addition

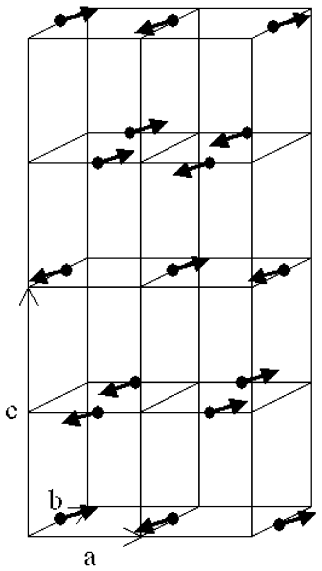

Figure 6. Schematic view of the magnetic structure of Sr_2CoWO_6. The chemical unit cell is doubled along *x* and *z*. Only Co ions and their magnetic moments (oriented along [110 directions] are represented.

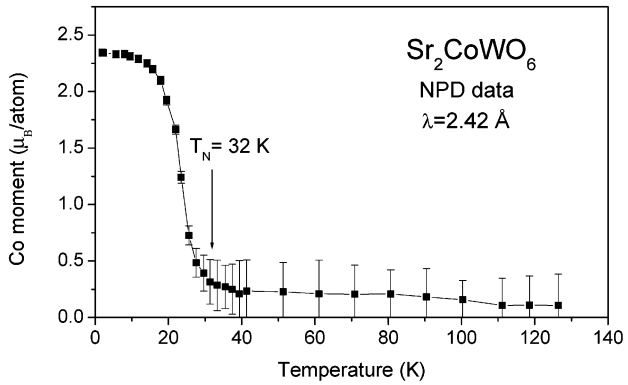

Figure 7. Thermal evolution of the ordered magnetic moment on Co positions refined from NPD data.

of two tilts in "anti-phase" in the *a* and *b* directions and a change from "anti-phase" to "in-phase" in the *c* direction. This addition of two new tilts along *a* and *b* is in agreement with the sharp contraction of the *c* axis and the decrease in volume below the phase transition.

DSC Data. DSC data in the 223−773 K temperature range are shown in Figure 11. Two endothermic peaks are observed at ca. 260 and 660 K (−13.3 and 386.4 °C). The first one is in agreement with the tetragonal to monoclinic phase transition observed with NPD measurements. The former probably corresponds to a tetragonal to cubic transition, at present not verified with diffraction data.

Magnetic Data. The magnetic susceptibility vs temperature data (Figure 12) shows a low-temperature maximum, at $T_N = 24$ K, corresponding to the transition to an antiferromagnetically ordered phase. The same Néel temperature had been reported for this compound.[13,14] The reciprocal susceptibility vs temperature plot (Figure 13) gives a perfect straight line. A Curie−Weiss fit above 200 K gives a paramagnetic moment of 5.20 μ_B, much larger than the spin-only value expected

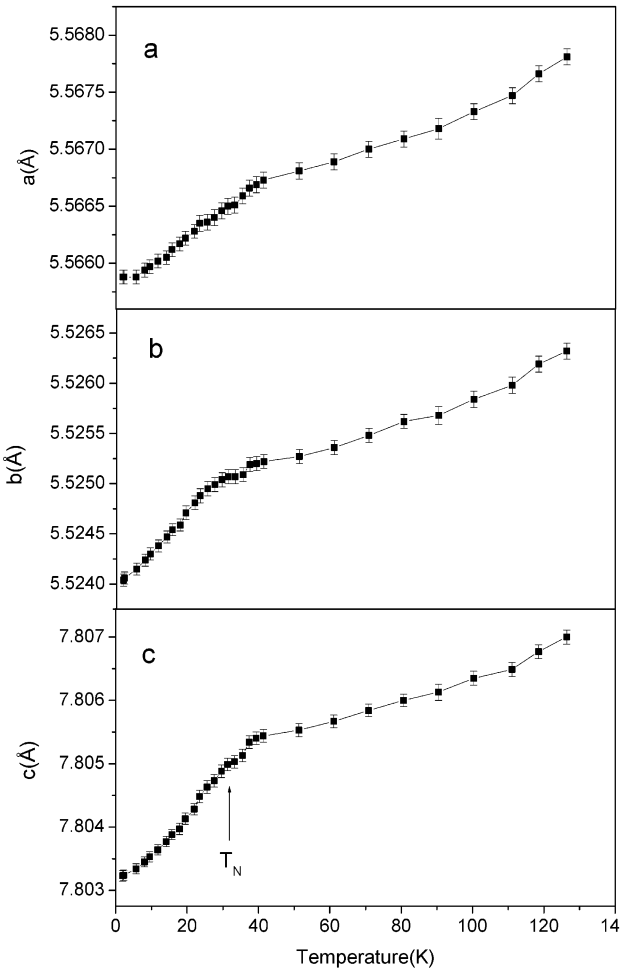

Figure 8. Dependence of cell parameters with temperature in the range 2−140 K.

for the couple Co^{2+}/W^{6+} (in any spin configuration for Co^{2+}). This point will be discussed in detail. The Weiss constant obtained is −62 K, confirming the presence of antiferromagnetic interactions in the paramagnetic region. The magnetization vs field plot at 2 K (Figure 14) gives a perfect straight line with no hysteresis, as expected for an antiferromagnet. No weak ferromagnetism effect or canting of the magnetic moments at low temperatures are observed. The difference between the Néel temperature obtained from susceptibility measurements (24 K) and that found from the NPD data (32 K) is probably due to a thermal hysteretic behavior of the much larger sample used for the neutron experiment, dynamically measured in the heating run. Transport measurements gave resistivities higher than 10^7 Ω-cm at RT; the thermal variation of the resistivity could not be measured.

Discussion

The perovskite structure ABO_3 consists of a tridimensional framework of vertex-sharing BO_6 octahedra, the voids of which are occupied by the more voluminous A cations. When A decreases in size, the BO_6 octahedra tilt to optimize A−O distances. The 23 different octahedral tilting systems were originally studied by Glazer,[21] and later on by O'Keefe and Hide.[22] More recently, Woodward[18] described the possible tilting systems for $A_2BB'O_6$ ordered perovskites, predicting the

(20) Brown, I. D.; Altermatt, D. *Acta Crystallogr. B* **1985**, *41*, 244.
(21) Glazer, A. M. *Acta Crystallogr. B* **1972**, *28*, 3384.

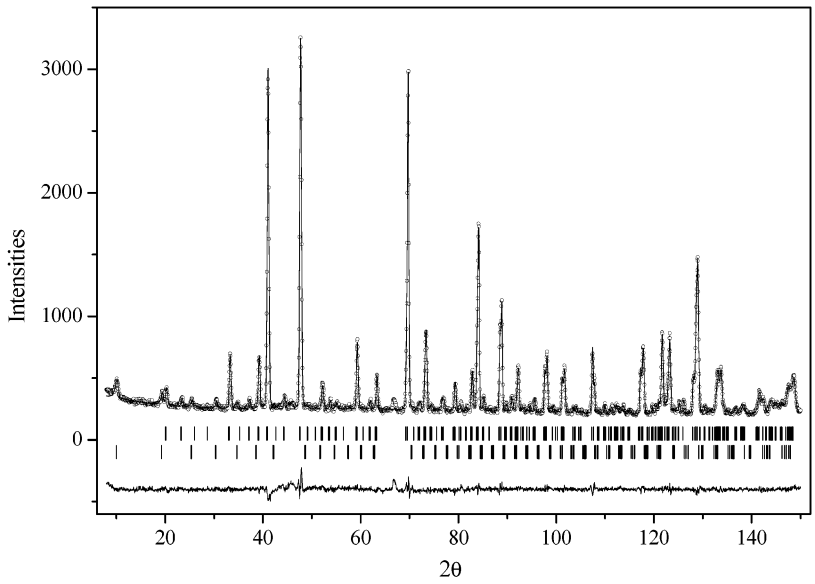

Figure 9. Observed (circles), calculated (full line), and difference (bottom) NPD Rietveld profiles for Sr_2CoWO_6 at 2 K. Vertical lines correspond to the Bragg positions for the crystallographic phase (top) and magnetic phase (bottom). For clarity, Bragg positions for impurity phases were omitted.

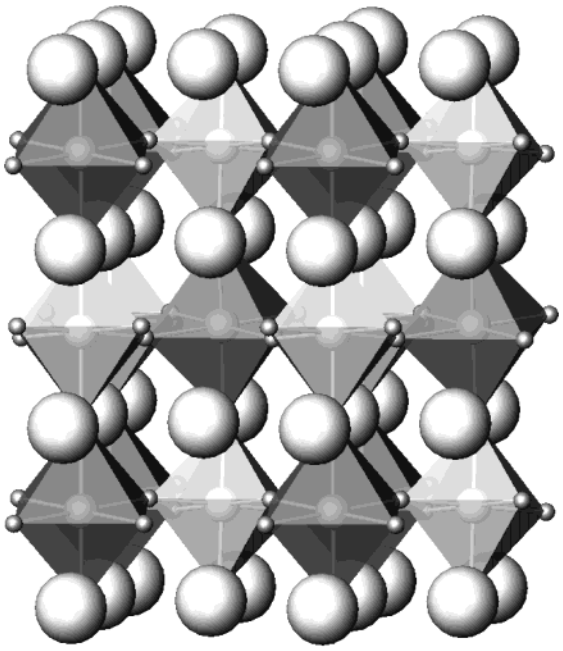

Figure 10. View of the structure of monoclinic Sr_2CoWO_6 at 2 K. *c* axis is vertical; *b* axis is from left to right. Large spheres represent Sr; small spheres represent O; corner-sharing CoO_6 (dark) and WO_6 octahedra are tilted with an $a^-a^-c^+$ scheme, to optimize Sr−O bond lengths.

space groups for each system. When the A cation is large enough, the well-known $(NH_4)_3FeF_6$ structure is adopted by 1:1 B-site ordered perovskites, such as Ba_2FeMoO_6, which can be described in the cubic space group $Fm\bar{3}m$. For slightly smaller A cations, only a slight deformation of the lattice takes place, implying the tilting of the octahedra only along the *c* axis. This tilting means a reduction in symmetry from cubic to tetragonal. Depending on the sign of the tilt, either in-phase ($a^0a^0c^+$ according to Glazer's nomenclature[21]) or anti-phase ($a^0a^0c^-$), two space groups describe the changes in symmetry: $P4/mnc$ in the first case or $I4/m$ in the second one.

The differences between both models are very subtle since they involve mainly small shifts of the in-plane oxygen atoms. These position changes can be difficult to detect by X-ray diffraction; hence, a NPD study is

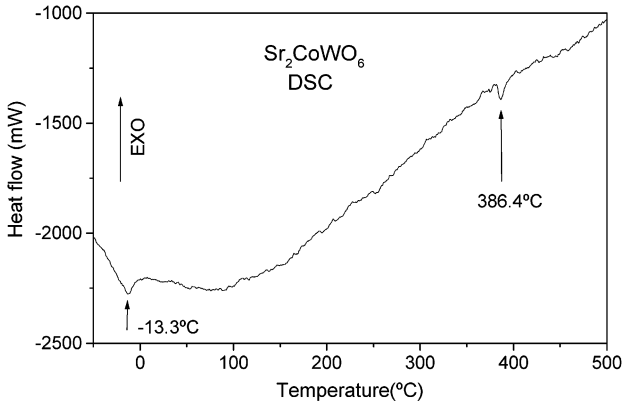

Figure 11. Differential scanning calorimetric measurement of Sr_2CoWO_6. The endothermic peak at −13.3 °C corresponds to the monoclinic (low temperature) to tetragonal (high temperature) crystallographic phase transition.

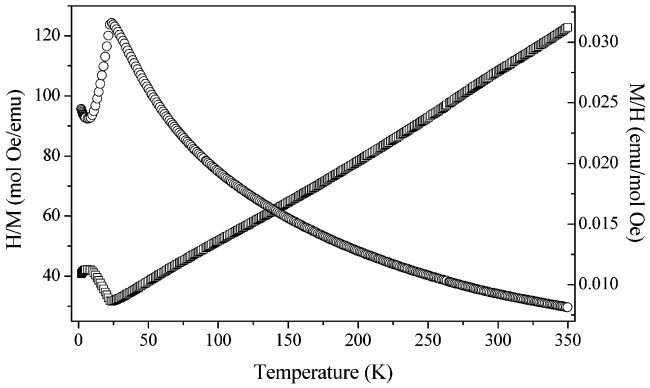

Figure 12. Magnetic susceptibility (χ) and reciprocal magnetic susceptibility (χ^{-1}) vs *T* for Sr_2CoWO_6 in the 4−350 K temperature range.

(22) O'Keeffe, M.; Hyde, B. G. *Acta Crystallogr. B* **1977**, *33*, 3802.

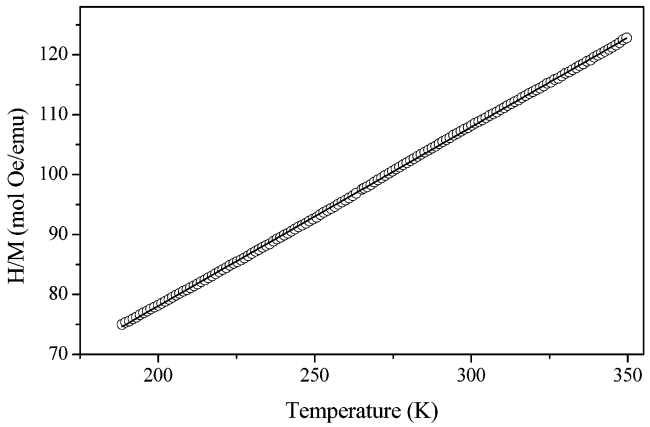

Figure 13. Curie−Weiss plot as the thermal variation of the reciprocal magnetic susceptibility (χ^{-1}) for Sr_2CoWO_6 in the 190−350 K temperature range.

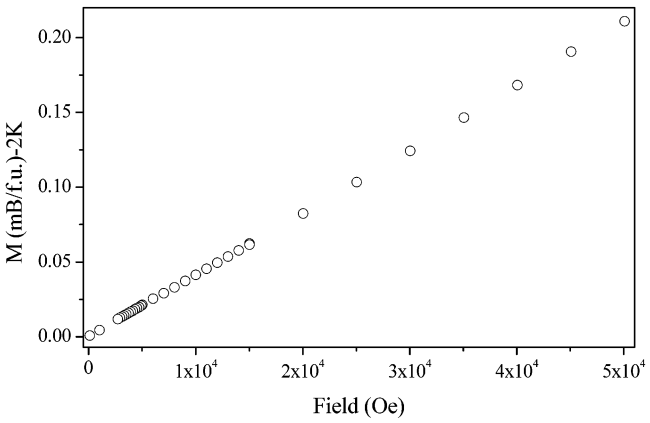

Figure 14. Magnetization vs field isotherm (T = 2 K) for Sr_2CoWO_6.

essential for investigation of these structural features since neutrons are more sensitive to the oxygen positions. Our room-temperature NPD study performed at the D2B diffractometer allowed us to determine the true space group: a trial refinement in *P*4/*mnc* led to a much worse fit of the data. The structure of Sr_2CoWO_6 can, thus, be described at room temperature as the result of a single anti-phase octahedral tilting along the *c* axis. Figure 3 illustrates this particular feature. The magnitude of the tilting can be simply derived from the Co−O2−W angle, to be 7.24°. CoO_6 and WO_6 octahedra are almost fully ordered and alternate along the three directions of the crystal, in such a way that each CoO_6 octahedra is linked to 6 WO_6 octahedra, as shown in Figure 3, and vice versa. The driving force for the Co/W ordering is the charge difference between both kinds of cations since the size difference is not too large. In Table 2 we notice that CoO_6 octahedra are slightly larger than WO_6 octahedra, being this in agreement with the difference in ionic radii.[23] CoO_6 octahedra are slightly elongated along the *c* axis, whereas WO_6 octahedra are slightly shortened along the *c* axis. The small deviation from cubic symmetry (measured as $c/(a2^{1/2}) = 1.010$) explains why this and many other double perovskites were informed as cubic or tetragonal with a smaller cell[11,14,15] in the 1960s and 1970s.

To obtain some insight into the oxidation states distributions, we carried out a series of bond-valence calculations by means of the Brown model.[19] This model gives a phenomenological relationship between the formal valence of a bond and the corresponding bond lengths. In perfect nonstrained structures, the bond-valence sum (BVS) rule states that the valence (V_{ij}) of the cation (anion) is equal to the sum of the bond valences (v_{ij}) around this cation (anion). Bond valences are calculated with the formula $v_{ij} = \exp[(R_{ij} - d_{ij})/0.37]$, where R_{ij} is the bond-valence parameter and d_{ij} is the anion−cation bond length. The valence of the atom i (V_i) is then calculated as $\sum v_{ij}$.

Bond-valence sums for all the ions are shown in Table 3. From these values the electronic configuration for this compound at 298 and 2 K should be $Co^{2+}(3d^7)-W^{6+}(5d^0)$, which accounts for the electrical insulating behavior of this sample. On the other hand, the large effective moment (5.2 μ_B) obtained in the paramagnetic region well above T_N is hardly compatible with this electronic configuration and a spin-only contribution. Even considering high-spin (H.S.) Co^{2+} ($S = {}^3/_2$), the total paramagnetic moment would be as low as 3.87 μ_B. High-spin octahedral Co^{2+} has a $^4T_{1g}$ ground state and, consequently, exhibits unquenched spin−orbital coupling[24] with an expected magnetic moment of 5.20 μ_B. This value is coincident with the experimental value, this being indicative of a regular or weakly distorted octahedral environment.

Unquenched magnetic contribution has also been observed for Co^{2+} in other compounds, that is, $BaLn_5CoS$ (Ln = La, Ce, Pr, or Nd)[25] (with Co^{2+} in tetrahedral coordination) and $[Ph_4P]_2\{Co^{II}[N(CN)_2]_4\}$,[26] $Sr_3CoSb_2O_9$,[27] and Sr_2CoMoO_6[12] (with Co^{2+} in octahedral coordination). Although similar magnetic moment values for Co^{2+} (4.90 $\leq \mu_B \leq$ 5.20) have been observed in other double perovskites such as Ba_2CoWO_6,[28] Pb_2CoWO_6,[29,30] Ca_2CoWO_6, $SrLaCoSbO_6$, $SrLaCoTaO_6$, Sr_2CoUO_6, and Sr_2CoMoO_6,[31] these values were not specifically assigned to unquenched orbital magnetic contributions. The reason this has been observed only in a few cases in perovskite oxides is that Co^{2+} is rather rare since it is only stabilized in double perovskites of the type $A_2Co^{2+}B^{6+}O_6$ (A = M^{2+}) and the octahedral environment has to be quite regular; otherwise, the orbital magnetic moment is quenched.

Co^{2+} can be found also in perovskite fluorides, that is, $ACoF_3$ (A = alkaline metal). Unquenched orbital contribution has been indeed observed in $KCoF_3$.[32,33]

(23) Shannon, R. D. *Acta Crystallogr. A* **1976**, *32*, 751.

(24) Mabbs, F. E.; Machin, D. J. *Magnetism and Transition Metal Complexes*; Chapman & Hall: London, 1973; pp 99−100.

(25) Wakeshima, M.; Hinatzu, Y. *J. Solid State Chem.* **2001**, *159*, 163.

(26) Raebiger, J. W.; Manson, J. L.; Sommer, R. D.; Geiser, U.; Rheingold, A. L.; Miller, J. S. *Inorg. Chem.* **2001**, *40*, 2578.

(27) Primo-Martín, V.; Jansen, M. *J. Solid State Chem.* **2001**, *157*, 76.

(28) Cox, D. E.; Shirane, G.; Frazer, B. C. *J. Appl. Phys.* **1967**, *38*, 1459.

(29) Bokov, V. A.; Kizhaev, S. A.; Myl'nikova, I. E.; Tutov, A. G. *Sov. Phys.-Solid State* **1965**, *6*, 2419.

(30) Kizhaev, S. A.; Bokov, V. A. *Sov. Phys.-Solid State* **1966**, *8*, 1554.

(31) Blasse, G. *Proceedings International Conference Magnetism*, Nottingham, 1964, Institute of Physics and the Physical Society: London, 1964; p 350.

(32) Suzuki, N.; Isu, T.; Motizuki, K. *Solid State Commun.* **1977**, *23*, 319.

(33) Tsuda, T.; Yasuoka, H.; Miyauchi, T. *J. Phys. Soc. Jpn.* **1978**, *45*, 1551.

As a measure of the octahedral distortion, the relation between the largest Co−O bond $(d\text{Co}-\text{O})_L$ and the shortest one $(d\text{Co}-\text{O})_S$ can be calculated. For Sr_2CoWO_6 from Table 2 we calculate $(d\text{Co}-\text{O})_L/(d\text{Co}-\text{O})_S = 1.013$ at 298 K and 1.008 at 2 K. For S_2CoMoO_6 this value is 1.000 (within the experimental error) and for $Sr_3CoSb_2O_9$ we calculate 1.007. All of them are almost completely regular, which accounts for the presence of an unquenched orbital magnetic moment in these compounds.

It is interesting to underline that the effective moment for Co^{2+} obtained in the paramagnetic region includes, as discussed, an unquenched orbital contribution, whereas the ordered magnetic moment obtained from NPD in the antiferromagnetic state is comparable with the spin-only contribution. In fact, the superexchange interaction field giving rise to the magnetic ordering is also responsible for the quenching of the orbital contribution, in such a way that only the spin contribution is observed in the antiferromagnetic region. Values of the magnetic moments obtained from NPD for some high-spin Co^{2+} compounds are always lower than the corresponding effective magnetic moments obtained from the Curie−Weiss law.[34] This difference between the paramagnetic moment obtained by the Curie−Weiss law and the magnetic moment obtained from neutron diffraction in the antiferromagnetic state has been specifically observed in the double perovskite Pb_2CoWO_6 by Cox et al.,[28] however not assigned to the orbital magnetic moment quenching by the magnetic ordering. It is interesting to notice that in the perovskite $KCoF_3$ there is no quenching of the orbital magnetic moment in the antiferromagnetic state.[33] Thus, the unquenched orbital contribution to the magnetic moment, which disappears upon entering the AFM state, is unique to the Co^{2+}-containing double perovskites.

The observed antiferromagnetic ordering can be understood from the magnetic interactions present in the crystal structure. There is a large variety of cobalt double perovskites showing a wide range of magnetic properties, for example, antiferromagnetism,[13,14] ferromagnetism,[35] spin-glass behavior,[27,36] and magnetoresistance,[12,37] depending on the respective composition. These magnetic properties are strongly influenced by the order−disorder of paramagnetic B cations. For example, when B cations are disordered (random distribution at the same crystallographic sites), spin-glass behavior is observed at low temperatures,[38−40] because the spins are "in conflict" with each other, that is, "frustrated", due to structural disorder in the solid. On the other hand, B-site ordered ones exhibit ferrimagnetism,[8,11] ferromagnetism[7,11] or antiferromagnetism.[11,12] When B′ is a nonmagnetic ion (W^{6+} in our case) and B and B′ are in different crystallographic sites (ordered B sites), an array of O−B′−O exists between every two magnetic B ions, and the superexchange interactions, even if weak, are still present. Consequently, an antiferromagnetic order is observed with a relatively low ordering temperature, as for the present case. The results of the bond-valence sums (Table 3) also account for the magnetic behavior since if the electronic configuration were $Co^{3+}(3d^6)-W^{5+}(5d^1)$ instead of $Co^{2+}(3d^7)-W^{6+}(5d^0)$, ferrimagnetic coupling between Co^{3+}(HS) (d^6, $S = 2$) and W^{5+} (d^1, $S = 1/2$) would have been expected.

Conclusions

Sr_2CoWO_6 perovskite is an insulating antiferromagnet ($T_N = 24$ K). At room temperature it has a tetragonal (space group $I4/m$) structure; the crystal contains alternating CoO_6 and WO_6 octahedra, tilted by 7.24° in the basal ab plane (Glazer notation $a^0a^0c^-$), as shown from NPD data. The effective magnetic moment calculated through the linear fit of the Curie−Weiss law at high temperatures (5.20 μ_B) indicates that the orbital contribution is unquenched at these temperatures, which is consistent with high-spin Co^{2+} ($^4T_{1g}$ ground state) in a quasi-regular octahedral environment. Variable temperature NPD and DSC data indicate a tetragonal (space group $I4/m$) to monoclinic (space group $P2_1/n$) structural transition at 260 K and variable temperature NPD and magnetic measurements indicate a transition to an antiferromagnetic ordered state at $T_N = 24$ K. The superexchange interaction field giving rise to the magnetic ordering is also responsible for the quenching of the orbital contribution, in such a way that only the spin contribution is observed in the antiferromagnetic region. At 2 K the structure contains alternating CoO_6 and WO_6 octahedra, tilted in-phase by 4.77° along the [001] direction of the pseudocubic cell and in anti-phase by 5.82° along the [010] and [100] directions ($a^-a^-c^+$ Glazer's notation). The results of the bond-valence sums, the antiferromagnetic properties, and the insulating behavior are consistent with an electronic configuration $Co^{2+}(3d^7)-W^{6+}(5d^0)$ instead of $Co^{3+}(3d^6)-W^{5+}(5d^1)$.

Acknowledgment. We are thankful for the financial support of CICyT (Spain) to the project MAT2001-0539 and MAT97-345 and Prof. Peter Stephens for providing us beam time at the SUNY X3B1 beamline of NSLS, Brookhaven National Laboratory, USA. J. C. Pedregosa and R. E. Carbonio acknowledge the financial support of the Consejo Nacional de Investigaciones Científicas y Técnicas (PID 4929/96 and PIP 380/98), the Agencia Nacional de Promoción Científica y Tecnológica (PICT98 06-03041 and PICT99 12-5378), Fundación Antorchas (collaboration project A-13740/1-94), CyT-Universidad Nacional de San Luis (Project 7707), and SECyT-UNC.

CM0208455

(34) Weast, R. C., Ed. *CRC Handbook of Chemistry and Physics*, 68th ed.; CRC Press Inc.: Boca Raton, FL, 1987−1988; p E-117.
(35) Kawasaki, S.; Takano, M.; Takeda, Y. *J. Solid State Chem.* **1996**, *121*, 174.
(36) Lappas, A.; Prassides, K.; Gygax, F. N.; Schenk, A. *J. Solid State Chem.* **1999**, *145*, 587.
(37) Maignan, A.; Martin, C.; Pelloquin, D.; Nguyen, N.; Raveau, B. *J. Solid State Chem.* **1999**, *142*, 247.
(38) Battle, P. D.; Gibb, T. C.; Herod, A. J.; Kim, S. H.; Hunns, P. H. *J. Mater. Chem.* **1995**, *5*, 75.
(39) Battle, P. D.; Gibb, T. C.; Herod, A. J.; Hodges, J. P. *J. Mater. Chem.* **1995**, *5*, 865.
(40) (a) Kim, S. H.; Battle, P. D. *J. Solid State Chem.* **1995**, *114*, 174. (b) Gibb, T. C. *J. Mater. Chem.* **1993**, *3*, 441.